water

MDPI

Article

Flood Extent Delineation and Exposure Assessment in Senegal Using the Google Earth Engine: The 2022 Event

Bocar Sy [1,*], Fatoumata Bineta Bah [1] and Hy Dao [2,3]

[1] Laboratory of Applied Geomatic (LAG), Department of Geoscience and Environment, Polytech Diamniadio, Université Amadou Mahtar Mbow, Rue 21*20, 2ème Arrondissement, Pole Urbain de Diamniadio, Dakar 15258, Senegal; bah.fatoumata@uam.edu.sn
[2] Department of Geography and Environment, Geneva School of Social Sciences, University of Geneva, 66 Boulevard Carl-Vogt, 1205 Geneva, Switzerland; hy.dao@unige.ch
[3] Institute for Environmental Sciences, University of Geneva, Boulevard Carl-Vogt 66, 1205 Geneva, Switzerland
* Correspondence: bocar.sy@uam.edu.sn

Abstract: This study addresses the pressing need for flood extent and exposure information in data-scarce and vulnerable regions, with a specific focus on West Africa, particularly Senegal. Leveraging the Google Earth Engine (GEE) platform and integrating data from the Sentinel-1 SAR, Global Surface Water, HydroSHEDS, the Global Human Settlement Layer, and MODIS land cover type, our primary objective is to delineate the extent of flooding and compare this with flooding for a one-in-a-hundred-year flood event, offering a comprehensive assessment of exposure during the period from July to October 2022 across Senegal's 14 regions. The findings underscore a total inundation area of 2951 square kilometers, impacting 782,681 people, 238 square kilometers of urbanized area, and 21 square kilometers of farmland. Notably, August witnessed the largest flood extent, reaching 780 square kilometers, accounting for 0.40% of the country's land area. Other regions, including Saint-Louis, Ziguinchor, Fatick, and Matam, experienced varying extents of flooding, with the data for August showing a 1.34% overlap with flooding for a one-in-a-hundred-year flood event derived from hydrological and hydraulic modeling. This low percentage reveals the distinct purpose and nature of the two approaches (remote sensing and modeling), as well as their complementarity. In terms of flood exposure, October emerges as the most critical month, affecting 281,406 people (1.56% of the population). The Dakar, Diourbel, Thiès, and Saint-Louis regions bore substantial impacts, affecting 437,025; 171,537; 115,552; and 77,501 people, respectively. These findings emphasize the imperative for comprehensive disaster preparation and mitigation efforts. This study provides a crucial national-scale perspective to guide Senegal's authorities in formulating effective flood management, intervention, and adaptation strategies.

Keywords: flood extent mapping; flood exposition assessment; remote sensing; Google Earth Engine; Sentinel-1; hydrological and hydraulic modeling

Citation: Sy, B.; Bah, F.B.; Dao, H. Flood Extent Delineation and Exposure Assessment in Senegal Using the Google Earth Engine: The 2022 Event. *Water* **2024**, *16*, 2201. https://doi.org/10.3390/w16152201

Academic Editor: Enrico Creaco

Received: 22 April 2024
Revised: 22 June 2024
Accepted: 27 June 2024
Published: 2 August 2024

1. Introduction

The anticipated impacts of climate change are set to exacerbate the frequency and severity of hydro-climatic extreme events, notably floods and droughts, in vulnerable regions like numerous African countries [1]. Among these events, floods stand out as being particularly prevalent and consequential in Africa [2]. Over the past two decades (2002–2022), floods have accounted for 64% of all disasters on the continent. During this period, Africa endured 793 flood disasters, resulting in over 16,900 fatalities, and adversely affecting the lives of 58 million people [3]. Senegal, in particular, has borne a significant burden from flooding, experiencing 13 flood events over the same period and impacting a substantial 23,874,963 individuals [3]. The consequences, beyond the loss of human life, extend to the destruction of farmland. Notably, the troubling trend of entire regions facing

inundation on a biennial basis is on the rise. This increase can be attributed to a confluence of factors, such as climate change, persistent poverty, and rapid urbanization [4,5].

The compounding effects of continuous socio-economic changes, including rapid urbanization and agricultural expansion [6,7], further elevate the exposure to flooding. These changes contribute significantly to the escalating flood risk, as evidenced by research by Hirabayashi [8]. In essence, the convergence of climate change and anthropogenic factors amplifies the challenges faced by regions like Senegal, necessitating a comprehensive understanding of escalating disaster risk and effective risk management strategies to safeguard both lives and livelihoods.

Although concerted mitigation efforts have been made by Senegalese authorities, involving the construction of retention basins, pipelines, pumping stations, and even the relocation of residents, the measures are insufficient [9,10]. A limiting factor is the absence of comprehensive mapping of flood exposure. Such mapping is crucial to precisely target spatially effective mitigation strategies, as emphasized by Li et al. [11], providing invaluable insights for government and disaster relief agencies.

The lack of comprehensive flood mapping prevents the visualization of regions susceptible to specific flood scenarios, as highlighted by Sy et al. [12]. Additionally, the absence of detailed flood mapping hampers exposure assessments of people and assets for a one-in-a-hundred-year flood event, a critical aspect emphasized by Muis et al. [13]. The lack of flood hazard and exposure mapping undermines the ability of authorities to implement targeted and efficient mitigation measures, hindering the overall efficacy of flood risk reduction initiatives. Addressing these knowledge gaps is paramount for enhancing the resilience of Senegal and ensuring that mitigation efforts align with the specific needs of the exposed population and for a one-in-a-hundred-year flood event.

Significant progress has been made in mapping floods and assessing exposure at both local and national scales, notably with the development of Earth observation systems equipped with increased revisit frequency and a higher spatial resolution, along with easy access to both satellite imagery and data from other sources [11,14]. The Google Earth Engine (GEE), launched in 2010, has evolved into one of the world's most extensive publicly accessible Earth observation catalogs, amalgamating data from satellites and other sources. The GEE functions as a geospatial data and image visualization and processing tool, providing access to a plethora of international and regional datasets within the integrated code editor. This data is complemented by cloud computing resources, facilitating the extraction of timely, precise, and high-resolution information about the Earth's surface. Access to the GEE is freely available for academic and scientific research purposes (https://earthengine.google.com/platform/, accessed on 21 June 2024).

The GEE boasts a vast geospatial data repository, encompassing regularly updated Sentinel-1 Ground Range Detected (GRD) data [14]. The Synthetic Aperture Radar (SAR) capability of Sentinel-1 makes it particularly valuable for flood extent mapping, as it offers frequent observations, even in adverse weather conditions [15]. Flooded areas appear dark in SAR images due to their low backscatter signal, enabling differentiation from other land cover categories like agriculture and built-up areas [16]. The availability of analysis-ready SAR datasets on the GEE is a significant advancement in remote sensing applications. The GEE dataset encompasses more than four decades of archived earth observation imagery, including SAR data [17], allowing the continuous monitoring of global water bodies and their dynamics, such as floods [11]. Many studies have used SAR images in the GEE to map flood areas [14,16,18–21]. While some studies focus on global flood exposure [11,22], there has been little attention paid to data-scarce and developing countries [23–25]. These limited flood exposure assessment studies primarily evaluate land cover classes, such as "urban areas", or solely rely on population mapping layers.

While prior studies, particularly in Senegal, have investigated spatiotemporal flood mapping, using remote sensing, citizen science, and multi-criteria modeling at the local scale [12,26,27], there is a lack of such research at the national scale. To address this gap, the Senegalese government, through the Projet de Gestion Integrée des Inondations au Sénégal

(PGIIS) project, has recently initiated a geographic information system (GIS) for mapping flooding for a one-in-a-hundred-year flood event and conducting flood hazard assessments at a national level using hydrological and hydraulic modeling [28]. Notably, none of these studies use the GEE. Furthermore, there is a notable absence of spatiotemporal exposure assessment studies. In addition, to our knowledge, no study has attempted to compare flooded areas derived from the GEE with flooding for a one-in-a-hundred-year flood event.

Our study contributes to the growing knowledge base on flood hazards by comparing the largest flooded areas obtained from the GEE with flooding for a one-in-a-hundred-year flood event, derived from hydrological and hydraulic models. Unlike other studies that often focus on the global scale or well-documented regions, we concentrate on the data-scarce region of Senegal. We incorporate detailed analyses of the population density, urban areas, and farmland, providing a comprehensive assessment of flood exposure. In contrast to other studies conducted in Senegal and recent national-scale initiatives, we utilize the GEE and Sentinel-1 imagery to map flooded areas, a novel approach in Senegal, to our knowledge. Additionally, we assess population, urban, and farmland exposure, marking the first study in Senegal to do so, as far as we are aware.

The novelty of this research lies in its comprehensive approach to flood mapping, leveraging the GEE platform to address the challenges associated with data scarcity and rapid analysis in regions like Senegal. This study integrates remote sensing techniques with hydrological and hydraulic modeling to provide a thorough assessment of the flood hazard. By combining these approaches, this study achieves a more nuanced understanding of flood dynamics, leveraging the strengths and complementarity of both methodologies. Remote sensing offers real-time or near-real-time data on the extent of flooding, while hydrological and hydraulic modeling provides insights into the underlying processes driving flood events. This integration allows for a more robust assessment of the flood hazard, considering both spatial and temporal dimensions.

Furthermore, the comparison between observed and modeled flooding extents not only validates the accuracy of the modeling approach, but also highlights areas of agreement or discrepancy between the datasets. Through this process, this study enhances confidence in the reliability of flood hazard assessments, providing stakeholders with valuable insights into the strengths and limitations of different methodologies.

Beyond simply mapping the extent of flooding, this research aims to identify priority zones for mitigation measures. By overlaying flood extent areas with global population data, and urban area and farmland information, this study pinpoints regions most in need of flood risk reduction interventions, particularly in data-scarce areas. This proactive approach to flood management goes beyond merely depicting flood hazards, it informs targeted mitigation strategies, thereby enhancing the resilience of communities and ecosystems to flood events. Such comprehensive analysis supports the development of effective and efficient flood management policies, ultimately contributing to sustainable and resilient development.

The extreme meteorological event in Senegal in 2022 was marked by significant flooding, primarily occurring during the rainy season from June to October. ANACIM's report [29] highlights unprecedented rainfall levels, up to 150% higher than historical averages, particularly affecting the Senegal and Gambia river basins. This led to widespread flooding, impacting communities, urban areas, and agriculture. Utilizing Sentinel-1 data, this study aims to analyze flood exposure dynamics under extreme weather conditions, providing insights for comparison with flooding for a one-in-a-hundred-year flood event.

This study seeks to: (1) employ a remote sensing method to map flooded areas for the four months of the 2022 event on a national scale using the GEE tool, (2) compare the most flooded areas over the four months with flooding for a one-in-a-hundred-year flood event derived from hydrological and hydraulic modeling, evaluating the accuracy of flood modeling in order to enable the prioritization of mitigation measures by region, and (3) evaluate exposure in terms of population, urban area, and farmland for the four months of the 2022 flood event.

2. Study Area

The GEE approach was applied to all 14 regions of Senegal, in West Africa (Figure 1). Situated between 12°8–16°41 N and 11°21–17°32 W, Senegal borders Mauritania (to the north), Mali (east), Guinea Bissau, and Guinea Conakry (south), and the Atlantic Ocean (west), boasting a coastline spanning 700 km. Encompassing an area of 196 722 km^2 [30], Senegal is home to approximately 18 million inhabitants as of 2023, with a population density of around 92 inhabitants per km^2 [31]. The terrain is predominantly flat, with nearly 75% of the landmass at an elevation of less than 50 m. The highest point, reaching 581 m above sea level, is situated in the southeastern foothills of the Fouta-Djalon Mountain [28].

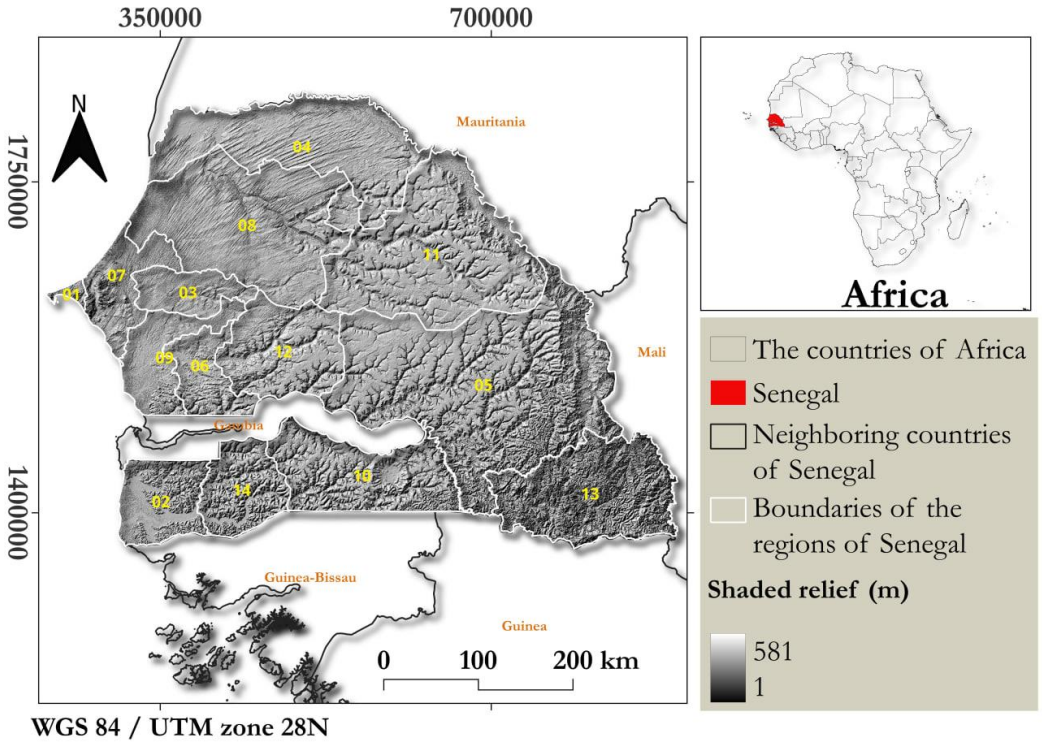

Figure 1. Location of the study area. The insert in the top right corner locates our study area on the African continent. The left-hand map represents our study area, Senegal, with 14 administrative regions, and shaded relief as the map background. The 14 regions are designated by numbers 1 to 14. The corresponding names are provided in Supplementary Table S1.

Senegal is administratively divided into 14 major regions (Decree No. 2013-10, Republic of Senegal). These regions feature a diverse range of landscapes. Urban centers, such as Dakar [1], Thiès [7], Kaolack [6], and Saint-Louis [4], play a crucial role in economic, cultural, and political spheres, with some urban regions containing rural areas as well. Similarly, certain rural regions like Ziguinchor [2], Fatick, Diourbel [3], Louga [8], Kolda [10], Matam [11], Tambacounda [5], Kédougou [13], Kaffrine [12], and Sédhiou [14], also include urban parts, albeit less developed. These cities and regions are characterized by bustling markets, modern infrastructure, and vibrant cultural scenes, or by agricultural and fishing activities in rural zones [32].

Senegal's climatic situation is characterized by two main seasons:

- The dry season (November to April/May) is marked by the prevalence of easterly maritime trade winds and westerly continental trade winds;
- The rainy season (June to October) is dominated by the monsoon flow from the St. Helena anticyclone.

The regions in Senegal have experienced frequent and significant flooding, resulting from various phenomena, for e.g., overflow flooding from perennial rivers, overflow flooding from temporary watercourses, urban runoff, rural runoff, flooding due to stagnation

in depressions or endoreic zones, and flooding due to rising groundwater. In some cases, these various phenomena combine and exacerbate the consequences.

3. Materials and Methods

3.1. Data

In this study, we utilized the GEE for all satellite data processing. The comparison of flooded areas with flooding for a one-in-a-hundred-year flood event was processed using ArcGIS Pro, including final map processing and layout. Microsoft Excel was employed for tabular data storage and histogram production. As outlined in Table 1, all the data layers were accessed from the GEE data catalog and processed within the GEE cloud computing platform [17]. Only the Senegalese administrative boundaries and the flooding for a one-in-a-hundred-year flood event were obtained from other sources. All raster and vector layers were saved in Senegal's coordinate system (UTM-28N (EPSG: 32 628)).

Table 1. An overview of the data layers used for the comparison between the flooded areas for a one-in-a-hundred-year flood event and flood exposure.

Layers Names	Sources	Date	Type	Resolution (m)
Administrative limits	LGA	2020	Vector	
Sentinel-1 images	Copernicus	Before flooding: 2–31 March 2022 After flooding: 20–31 July 2022; 1–31 August 2022; 1–10 September 2022; 1–10 October 2022	Raster	10
Flooding for a one-in-a-hundred-year flood event	PGIIS	2023	Raster	
Global Surface Water	EC/JRC	1 January 2022	Raster	30
HydroSHEDS	WWF US	22 February 2020	Raster	30
Global Human Settlement Layer	EC/JRC	2020	Raster	100
MODIS Land Cover Type	NASA	30 September 2022	Raster	500

The methodology employed in this study for the extent and exposure of the flooding for the 2022 flood event, follows the United Nations' recommended guidelines for flood mapping and exposure assessment using Sentinel-1 SAR data within the Google Earth platform (https://www.un-spider.org/advisory-support/recommended-practices/recommended-practice-google-earth-engine-flood-mapping/step-by-step, accessed on 22 June 2024).

To begin, we conducted monthly flood mapping using remote sensing techniques, at a spatial scale of 10 m during the wet season (July to October).

This was achieved by utilizing Sentinel-1 radar data to leverage both the available temporal resolution and the duration of the 2022 flood event (see Table 1), the 1984–2022 Global Surface Water (GSW) layer to identify the surface water distribution, and the 2020 HydroSHEDS layer. Finally, we assessed the flood exposure by integrating the flooded areas using remote sensing with the MODIS land cover type (MCD12Q1) version 6.1 data and layers depicting the population distribution and density, which were obtained from the Global Human Settlement Layer version P2023A (2020) in the GEE (Figure 2).

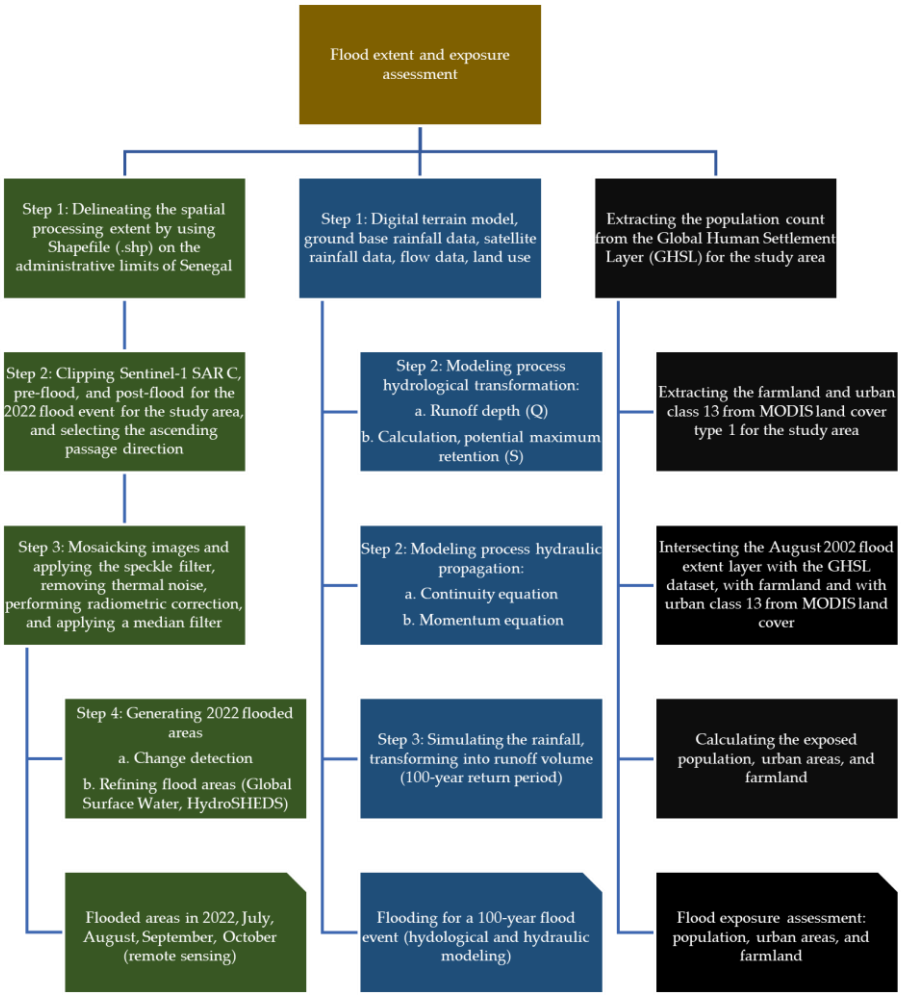

Figure 2. Framework for flood extent delineation and flood exposure assessment: remote sensing methodology (green), flooding for a one-in-a-hundred-year flood event methodology using modeling (blue), and methodology for estimating exposed population, urban areas, and farmland (black).

3.2. Mapping the Spatial and Temporal Distribution of Flooded Areas

To obtain information on the flooded areas using Sentinel-1 on the Google Earth Engine, we followed a four-step process (see green boxes in Figure 2).

Step 1: Specification of the study area.

This initial step involved defining the geographical boundaries for our study area. This information served to constrain the processing area, thus preventing unnecessary computations. To delineate the extent of the spatial processing, we utilized a Shapefile (.shp), depicting the administrative limits of Senegal for the 14 regions. This administrative boundary layer for Senegal was extracted from the Laboratory of Applied Geomatics (LGA) at Amadou Mahtar Mbow University.

Step 2: Timeframe and sensor parameters.

In addition to defining the area of interest, we specified the pre-flood and post-flood periods for each month of flooding (July, August, September, and October), as outlined in Table 1. We used Sentinel-1 SAR C-band (5.4 GHz) data provided by the European Space Agency (ESA) [33]. These images are acquired at intervals of at least every 6 or 12 days for each point on the globe, depending on the availability of Sentinel-1 imagery [34]. With a spatial resolution of 10 m, we accessed and clipped the level 1 GRD processed product in the GEE for the study area during the pre-flood and post-flood period (see Table 1). For our analysis, we chose vertical–horizontal (VH) polarization over vertical–vertical (VV) polarization. 'VH' polarization is widely recommended for flood mapping [16,35,36],

because it is more sensitive to changes on the ground surface, while 'VV' polarization is more sensitive to vertical structures and can be useful for delineating open water from the ground surface (e.g., detecting the coastline or a large expanse of water that has appeared after a flood).

Passage direction refers to the satellite's trajectory as it captures images, which can be either ascending (moving northward) or descending (moving southward). Consistency in the passage direction is crucial when detecting changes, as different viewing angles can create false positive signals. Globally, some areas are covered only by ascending or descending passage directions [37], while others are covered by both. For our study, we selected the ascending passage direction, which aligns with our study area. This ensures that the images being compared are consistent and reliable.

Step 3: Mosaicking images and applying the speckle filter.

This step involves sharpening the images before and during the flooding period, by removing thermal noise and performing a radiometric correction. We applied a 3 × 3 pixel median filter to remove the speckle effects in the SAR images, resulting in smoother images [36,38]. The median filter works as follows:

$$I'(\mathrm{x},\mathrm{y}) = median\{I(\mathrm{x}+i, y+j) | -1 \leq i, j \leq 1\}$$

where I′(x,y) is the output image, I(x,y) is the input image, and the median is calculated over a 3 × 3 window centered on each pixel (x,y). This process replaces each pixel value with the median value of its 3 × 3 neighbors, effectively reducing speckle noise.

Step 4: Generation of flooded area maps.

This step is divided into two parts.

Step 4a: Change detection.

In the first part, we aimed to detect changes between the pre- and post-flooding layers, which compare the before-flood and after-flood mosaics using the following algorithm:

$$\text{Change} = \frac{\text{After} - \text{flood mosaic}}{\text{Before} - \text{flood mosaic}}$$

A difference layer is created, upon which thresholding is applied (a threshold of 1.25; pixels above 1.25 assigned a value of 1; pixels below 1.25 assigned a value of 0) [36,38]. The binary change detection can be expressed as:

$$\text{Binary change} = \{1\ if\ change\ > 1.25, 0\ if\ change \leq 1.25\}$$

The resulting binary raster layer represents the potential flooded areas.

Step 4b: Refining the flooded areas.

In the second part, we intersected the generated binary layer with the GSW layer to exclude permanent water (water present for more than 10 months, e.g., lakes). This dataset, with a 30 m resolution, was extracted from the European Commission's Joint Research Center (EC/JRC). It contains maps of the location and the temporal distribution of surface water from 1984 to 2018 and provides statistics on the extent and evolution of surface water across the globe. The data were clipped to our study area.

Finally, we used the digital elevation model (DEM) layer to remove areas with a slope greater than 5%, as these areas are rarely flooded [12]. This raster layer was obtained from the Shuttle Radar Topography Mission within HydroSHEDS, which offers a suite of georeferenced rasters in tiles at a resolution of 30 m and mosaicked to cover the entire country.

The resulting layer represents the flooded areas. The flood extent was computed as follows:

$$\text{Flood extent} = \text{pixel area} * \text{number of pixels}$$

The area for each pixel is calculated in square meters.

3.3. Comparison of the Flooding for a One-in-a-Hundred-Year Flood Event with Flooded Areas Mapped Using Sentinel-1 Images, GSW Layers, and the DEM

The flooding for a one-in-a-hundred-year flood event was determined through hydrological and hydraulic modeling. This modeling was commissioned by the Senegalese Government through the PGIIS project.

3.3.1. Hydrological and Hydraulic Modeling

The proposed methodology consists of two steps (see blue boxes in Figure 2).

Step 1: Hydrological and hydraulic modeling data.

The flood inundation modeling was conducted using several datasets, as follows:

- Digital terrain model (DTM): Utilized Vricon's 2 m × 2 m resolution from Maxar Technologies, covering Senegal. This DTM, derived from high-resolution satellite imagery, integrates over a decade of monoscopic image collections from various angles;
- Ground-based rainfall data sourced from the World Meteorological Organization (WMO), the Hydrometric Information System for the Environment and Water Resources (SIEREM), and the National Agency of Civil Aviation and Meteorology (ANACIM): The WMO data include 59 stations covering 1900–2021, with a 71% gap rate, reduced to 50% for 1970–2021. The SIEREM data comprises 329 stations, with 181 stations having data from 1980–2007 and a 52% gap rate. The ANACIM data, with 23 stations providing data from 1955–2005;
- Satellite rainfall data: Integrated rainfall data from Integrated Multi-satellite Retrievals/Global Precipitation Measurement (IMERG/GPM; 2000–2020), Precipitation Estimation from Remotely Sensed Information using Artificial Neural Networks (PERSIANN; 2000–2019), Multi-source Weighted-Ensemble Precipitation (MSWEP; 1979–2017), Tropical Applications of Meteorology using SATellite and ground-based data (TAMSAT; 1983–2016), and Climate Hazards Group InfraRed Precipitation with Station data (CHIRPS; 1981-present), covering the study area, with various temporal and spatial resolutions;
- Flow data: Historical flow records incorporated to ensure model robustness, focusing on a 100-year return period flow;
- Land use information: Land use and soil characteristics data are crucial for modeling. Data sources include the Directorate of Geographic and Cartographic Works (DTGC) for detailed built-up area delineation, ESA Copernicus for land use data, the Institute of Research for Development (IRD) Soil Map for comprehensive soil mapping of Senegal, and the United States Geological Survey (USGS) Geologic Provinces of Africa (version 2.0) for geological zoning data.

Step 2: The modeling Process.

The second step describes the process of the model. This modeling process utilized HEC-RAS 6.5 software, employing 2D geometry for hydrological transformation and hydraulic propagation.

- Hydrological transformation: The Soil Conservation Service (SCS) method was applied, dynamically adjusting soil saturation levels and converting precipitation into runoff based on land use, soil type, and moisture conditions.

  a. Runoff depth (Q) calculation:

$$\mathrm{Q} = \frac{(\mathrm{P} - 0.2\mathrm{S})^2}{P + 0.8S}$$

  where Q = runoff depth (inches or mm); P = rainfall depth (inches or mm); SS = potential maximum retention after runoff begins (inches or mm), which is related to the curve number (CN).

  b. Potential maximum retention (S):

$$\mathrm{S} = \frac{1000}{CN} - 10$$

where CN = curve number, which is a dimensionless parameter related to the land use, soil type, and moisture conditions.

- Hydraulic propagation: Employed the Barré de Saint-Venant equations to simulate water movement, considering momentum conservation, continuity, and flow resistance.

  a. Continuity equation:

$$\frac{\partial \mathrm{A}}{\partial \mathrm{t}} + \frac{\partial Q}{\partial x} = 0$$

  where A = cross-sectional area of the flow (m^2); Q = flow rate (m^3s^{-1}); T = time (s); x = distance along the channel (m).

  b. Momentum equation:

$$\frac{\partial \mathrm{Q}}{\partial \mathrm{t}} + \frac{\partial}{\partial x}\left(\frac{Q^2}{A} + gA\frac{\partial y}{\partial x} + gA\left(S_O - S_f\right)\right) = 0$$

  where Q = flow rate (m^3s^{-1}); t = time (s); x = distance along the channel (m); g = acceleration due to gravity (9.81 ms^{-2}); y = flow depth (m); So = bed slope (mm^{-1}); Sf = friction slope (mm^{-1}).

- A synthetic rainfall event was simulated, represented as NetCDF rasters, depicting a concentrated 10-day rainfall episode within a 2-month period. The rainfall data was transformed into runoff volumes, representing a 100-year return period, and was used to produce flood maps for rare events.

This methodology enables the comprehensive mapping of flood-prone areas by simulating 2D water flows across the entire Senegalese territory. The model captures the overflow of watercourses of all sizes and accounts for runoff or accumulation in natural depressions. The outcome is a detailed representation of flood zones for a rare event, with an approximate return period of 100 years.

3.3.2. Comparative Analysis

In the comparative analysis, we juxtaposed the flooding for a one-in-a-hundred-year flood event delineated by the hydrological and hydraulic models, with flooded areas derived from Sentinel-1 using the GEE platform. This comparison had two primary objectives: first, to evaluate the accuracy of flood modeling in Senegal and, secondly, to facilitate the prioritization of mitigation measures by identifying regions where the two approaches overlap the most. To enhance the accuracy assessment, we employed spatial analysis techniques within ArcGIS Pro, specifically utilizing spatial join and zonal statistics tools. These tools facilitated the comparison between the boundary layers of the regions, the flooded areas obtained from the GEE, and the flooding for a one-in-a-hundred-year flood event predicted by hydrological and hydraulic models.

3.4. Estimation of Flood Exposure

3.4.1. Exposed People

To estimate population flood exposure across Senegal's 14 regions, in the GEE we utilized the Global Human Settlement Layer from the (EC/JRC) [39]. This layer with a resolution of 100 m and which was last updated in 2020, provides information on the population count per cell (see black boxes in Figure 2). Since our analysis was conducted at a 30 m resolution, we resampled this raster layer to match it using nearest neighbor interpolation. To avoid multiple counting of the population for the approximately $8 \times 8 \times 30$ m cells within the 100 m cells when using nearest neighbors, the approach is to allocate the 100 m population to 30 m cells using HydroSHEDS data. This ensures that each person is counted only once, regardless of how many smaller cells overlap with the larger 100 m cells. This method helps to maintain the accuracy of population counts and avoids overestimation due to double counting.

To integrate flood extent layers for the months of July, August, September, and October 2022 with the population data, we first reprojected the flood area rasters to align with the resolution and projection of the population dataset. Next, we conducted a spatial intersection between each flood extent layer and the population dataset, resulting in the creation of new raster layers. Finally, to calculate the total number of individuals exposed to flooding (see black boxes in Figure 2), we added up the pixel values within the exposed population raster.

3.4.2. Exposed Farmland and Urban Areas

To estimate the extent of exposed farmland, we utilized the MODIS land cover type (MCD12Q1) version 6.1 product, which offers a spatial resolution of 500 m and is updated annually. Given that our analyses were conducted at a 30 m resolution, we resampled the land cover raster to match it using nearest neighbor interpolation. This dataset is currently the only global dataset on land cover available in the GEE data catalog. Within the Land Cover Type 1 band, there are 17 classes, including two relevant farmland classes: class 12, indicating areas with at least 60% cultivation, and class 14, representing farmland/natural vegetation mosaics where small-scale cultivation occupies 40–60% of the area, alongside natural trees, shrubs, or herbaceous vegetation.

To identify exposed farmland, we extracted these farmland classes from the MODIS dataset and intersected them with the flooded areas in July, August, September, and October 2022 (see black boxes in Figure 2), which were resampled to match the scale and projection of the MODIS layer. Similarly, we calculated the areas of the affected urban and rural regions, using the same methodology applied to the flooded areas.

To identify exposed urban areas, we extracted the 'Urban Class 13' (see black boxes in Figure 2) from the 'Land Cover Type 1' band of the MODIS dataset. It is worth noting that during this process, the estimation of affected urban areas may be conservative due to challenges in detecting water within built-up areas, potentially leading to underestimation.

4. Results

4.1. Mapping of Flooded Areas Using Sentinel-1 Images, GSW Layers, and the DEM

We obtained the extent of the floods for the months of July, August, September, and October 2022, in Senegal, using Sentinel-1 images on the GEE platform. The methodology is described in Figure 2. We determined a total inundation area of 2951 km^2. It is noteworthy that during this event, all regions of the country experienced flooding at least once (Figures 3 and 4, Supplementary Material Table S2).

Further analysis indicates that August 2022 witnessed the most widespread flooding, covering 779.54 km^2 or 0.40% of the country's total surface area. September and July 2022 followed closely with, respectively, 746.80 km^2 and 723.98 km^2 or 0.38% and 0.37%, while September 2022 experienced the smallest extent of the flooding, encompassing 700.68 km^2 or 0.36% (Figures 3 and 4, Supplementary Material Table S2).

A closer look at the regions flooded shows that the Saint-Louis [4], Ziguinchor [2], Matam [11], and Fatick [9] regions recorded the most extensive flooding (Figures 3 and 4, Supplementary Material Table S2), with a mean area of 253.06, 93.55, 74.24, 86, and 70.75 km^2, respectively. These areas correspond to approximately 1.31%, 1.27%, 0.25%, and 1.03% of the respective total land area in these regions.

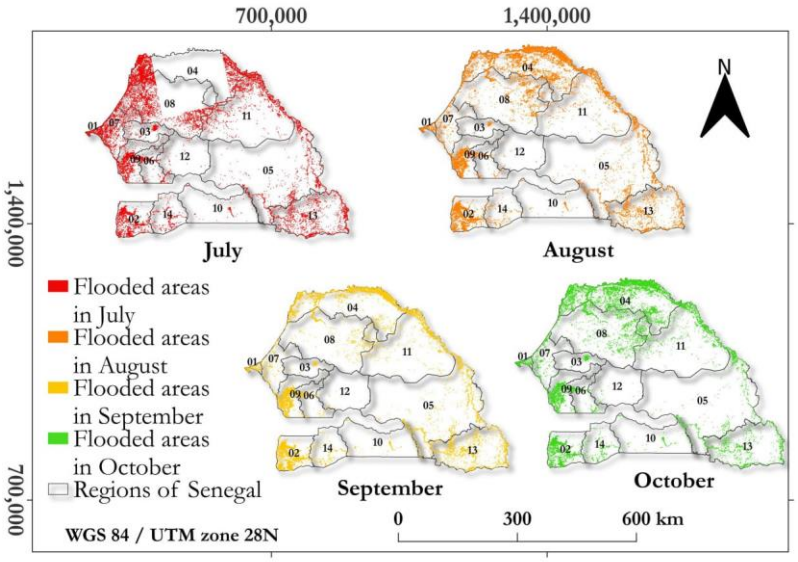

Figure 3. Spatial distribution of flooded areas based on Sentinel-1, GSW, and HydroSHEDS data for the 2022 flood event per region and month: July (red), August (orange), September (yellow), and October (light green).

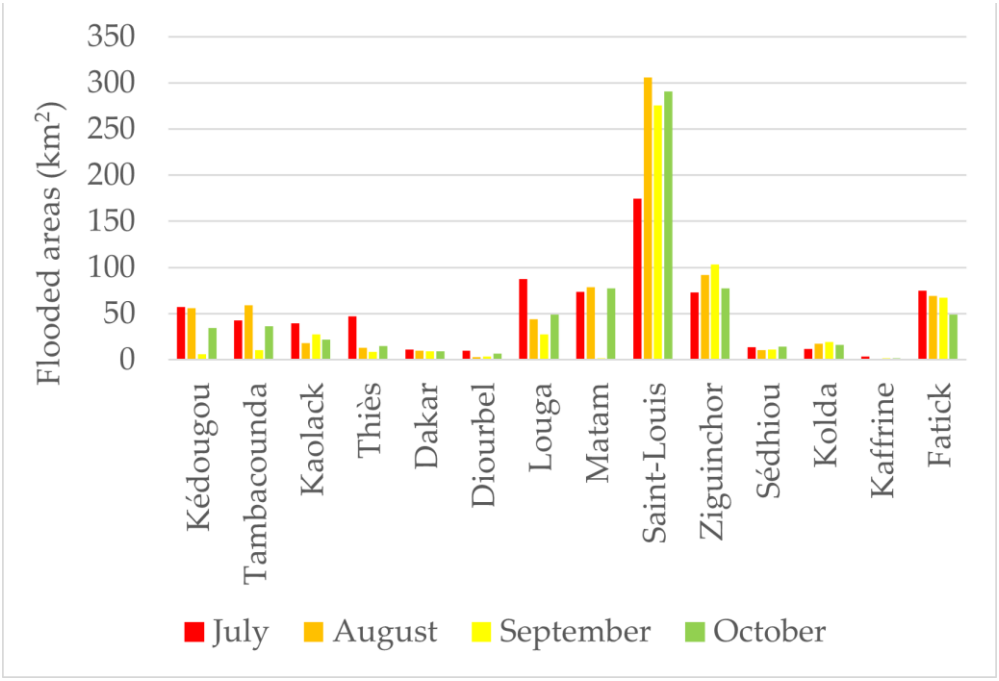

Figure 4. Histogram of flooded areas based on Sentinel-1, GSW, and HydroSHEDS data for the 2022 flood event per region and month: July (red), August (orange), September (yellow), and October (light green).

In terms of mapping, slight differences appear between the spatial location of the flooded areas for the month of July, August, September, and October 2022, showcasing variations of 8% (Figure 4). The GEE shows that in the Saint-Louis [4] region, the main flooded areas were in the northwest, northeast, and northern parts, but some flooded areas occurred in the central part and in the southeast (Figure 5). In the Ziguinchor [2] region, the main flooded areas were in the central and upper parts in low-lying areas, but some residual flooded areas were also found in the northwest and southeast (Figure 5).

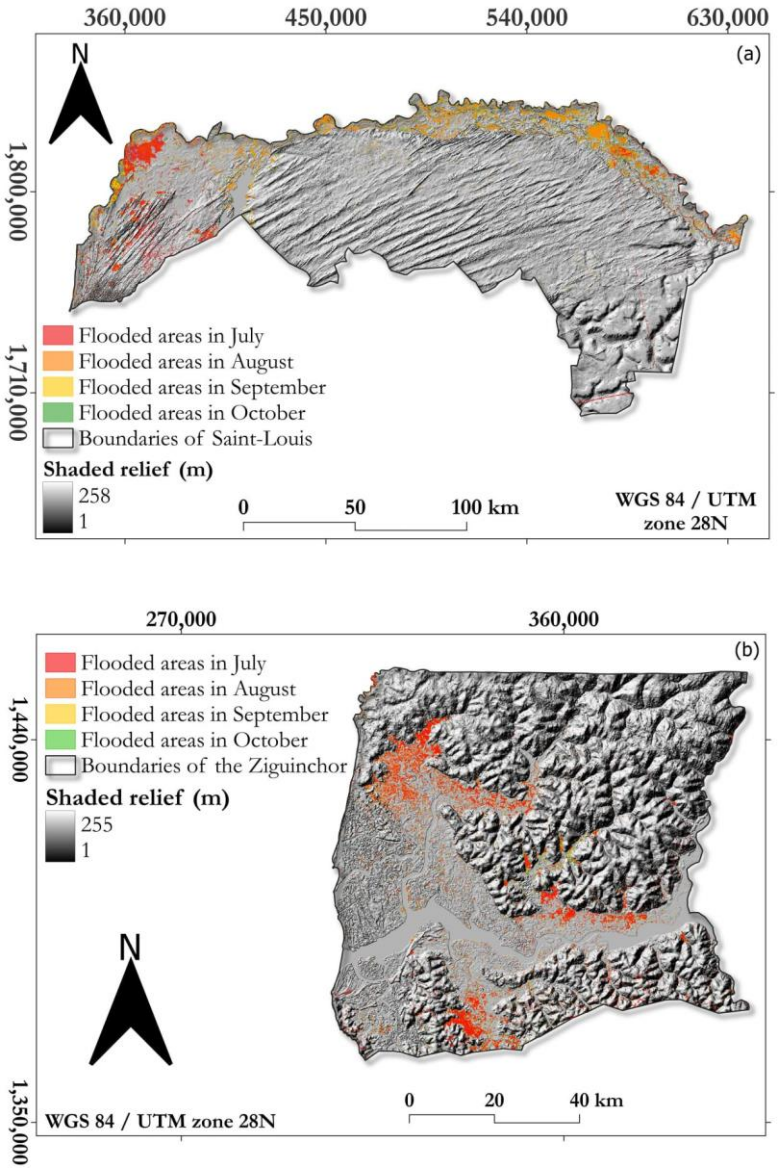

Figure 5. Spatial distribution of flooded areas based on Sentinel-1, GSW, and HydroSHEDS data for the 2022 flood event in the two most flooded regions: (**a**) Saint-Louis [4] (**top**) and (**b**) Ziguinchor [2] (**bottom**).

4.2. Comparison of Flooded Areas Obtained by Remote Sensing (Google Earth Engine) with 100-Year Flood-Prone Areas Obtained Using Hydrological and Hydraulic Modeling

The data obtained through the Google Earth Engine approach revealed that the flooding in the month of August 2022 was the most widespread, whereas the month of September 2022 was the smallest (Figures 3 and 4). The data obtained in August 2022 through the GEE approach was compared with hydrological and hydraulic modeling from the PGIIS project. The flooded areas in August 2022 provided by the GEE were smaller than those indicated by the modeling of the 100-year flood event (Table 2), showing a total overlap of only 1.43% across all 14 regions of the country, ranging from 0.04% in the Kaffrine [12] region to 10.19% in the Dakar [1] region (Table 2).

In terms of mapping, major differences emerge between the flood extent identified by remote sensing for the August 2022 flood event and the hydrological and hydraulic modeling, with spatial overlaps varying from one region to another. The analysis of these overlaps in the Dakar [1] region is shown in Table 2, with significant divergences. The total

area provided by remote sensing is approximately 18× smaller than that provided by the 100-year hydrological and hydraulic models of Senegal.

Table 2. Flooded areas obtained from the Google Earth Engine (remote sensing) in August 2022 in the second column and floodable areas from the PGIIS project (hydrological and hydraulic modeling) in the third column, with the percentage of overlapping areas between the remote sensing and hydrological and hydraulic modeling in the fourth column.

Administrative Region	Flooded Area (August 2022) from Remote Sensing (km^2)	Floodable Areas from Modeling (km^2)	Overlap (%)
Dakar	10.34	101.42	10.19
Ziguinchor	91.91	2992.43	3.07
Diourbel	2.99	1093.56	0.27
Saint-Louis	309.2	9666.56	3.20
Tambacounda	59.21	9739.77	0.61
Kaolack	18.31	1476.10	1.24
Thies	14.15	1313.32	1.08
Louga	41.14	6031.24	0.68
Fatick	69.1	3059.26	2.26
Kolda	18.17	2578.36	0.70
Matam	77.41	9449.34	0.82
Kaffrine	1.04	2631.82	0.04
Kedougou	56.22	2740.52	2.05
Sedhiou	10.53	1662.70	0.63
Total	779.54	54,536.34	1.43
Standard deviation			2.49

The remote sensing results show that the Saint-Louis region [4] was the most flooded during the 2022 flood event (309.02 km²). However, the Tambacounda region [5] (9739.77 km²) would be flooded more during the one-in-a-hundred-year flood event (Table 2).

To ensure the robustness of our comparison, we have included the standard deviation (σ) of the overlap (1.34%) between the flood extent derived from remote sensing and the floodable areas indicated by the modeling process. The σ value of 2.49% indicates a moderate level of variability in the overlap (1.34%). This variability can be attributed to differences in the spatial resolution of the datasets, the accuracy of remote sensing techniques in detecting water bodies, and the assumptions made in the hydrological and hydraulic modeling. By including this additional statistical measure, we provide a more comprehensive understanding of the reliability and consistency of our flood extent estimates, highlighting the areas where the remote sensing and modeling agree or diverge.

4.3. Exposed Population Assessment

Flood exposure was estimated using the intersection of the flooded areas from the Sentinel-1, GSW, HydroSHEDS, and the GHLS population layers. We estimated that around 782,681 people (4.35% of the Senegalese population) were exposed. The results show that October 2022 had the greatest population exposure by month, with 281,406 people exposed (1.56% of population). The lowest population exposure was estimated in August 2022, with 251,782 people exposed (1.39% of population) (Figure 6, Supplementary Material Table S3). The month with the highest exposure, October 2022, does not correspond to the month with the largest flooding extent (August 2022). The population exposure, estimated using the GHLS dataset, was greater in the Dakar [1], Diourbel [3], Thies [7], and Saint-Louis [4] re-

gions with, respectively, about 437,035 (11.22% of the Dakar [1] population), 171,837 (8.26% of the Diourbel [3] population), 115,552 (13.12% of the population in Thies), and 77,501 people exposed (6.2% of the population in Saint-Louis [4]) (Figure 6, Supplementary Material Table S3).

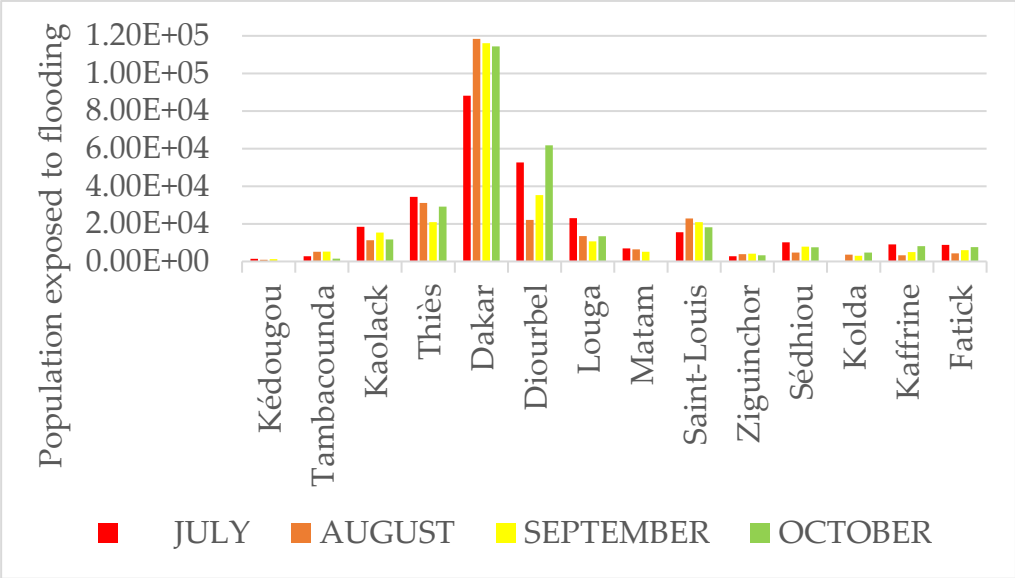

Figure 6. Population exposed to flooding from July to October 2022, estimated using the intersection of GHLS population datasets with the flooded areas in the Google Earth Engine.

Figure 7 presents spatial analysis of the flood exposure in Dakar [1] and Diourbel [3]. In the Dakar [1] region, the southeast area exhibits the highest concentration of people exposed to flooding. Conversely, in the Diourbel [3] region, the northwest part demonstrates the highest exposure of people to flooding.

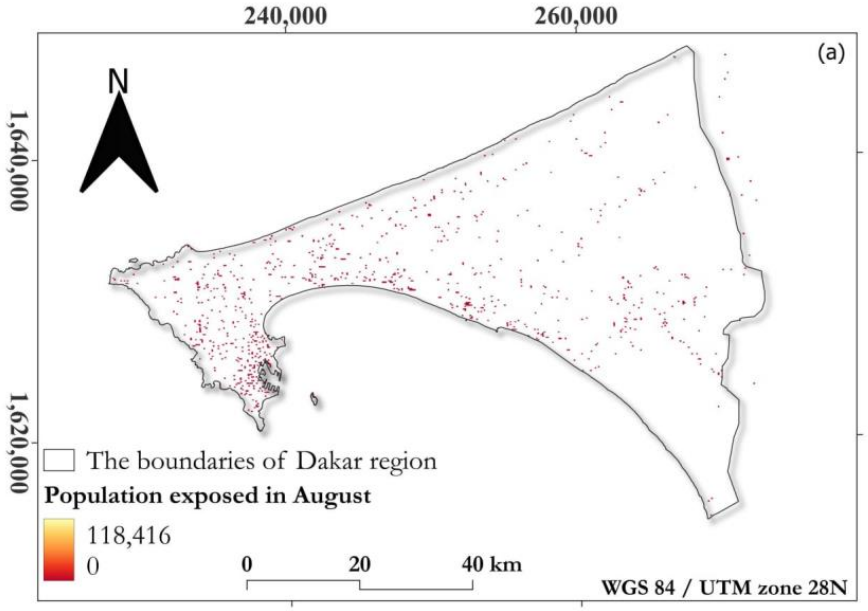

Figure 7. *Cont.*

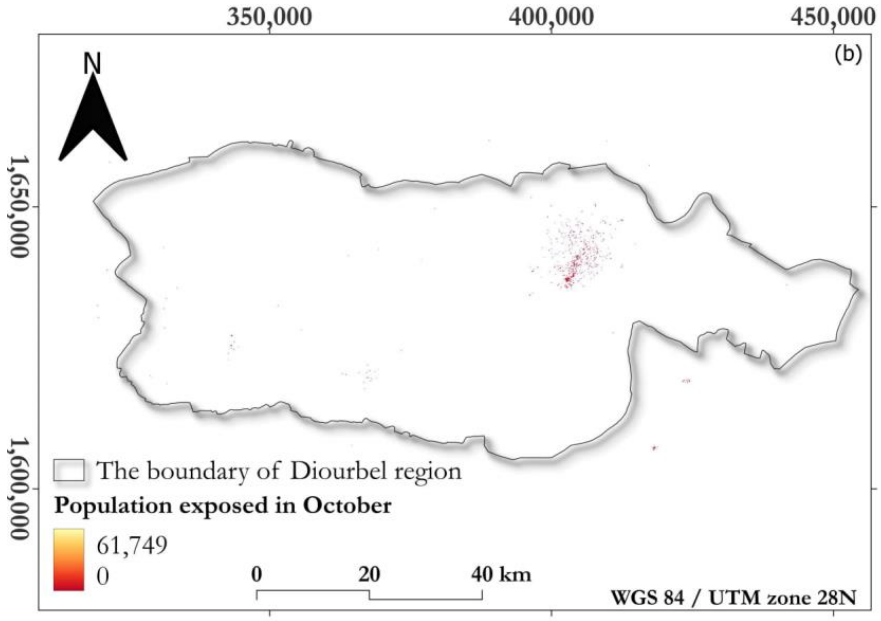

Figure 7. Spatial distribution of the two most exposed regions to flooding by population: (**a**) Dakar and (**b**) Diourbel. Assessed through the intersection of GHLS population datasets with the flooded areas in the Google Earth Engine.

4.4. Exposed Urban Areas and Farmland

Analysis of the 2022 flood event showed that a total of 238 km^2 (10.27%) of urban areas and 21 km^2 of farmland (1.37%) were exposed to flooding. The regions of Dakar [1], Diourbel [3], and Saint-Louis [4] have the highest amount of urban areas exposed to flooding. While the regions of Saint-Louis [4] and Thies [7] have the highest amount of farmland exposed to flooding (Figure 8, Supplementary Material Table S4).

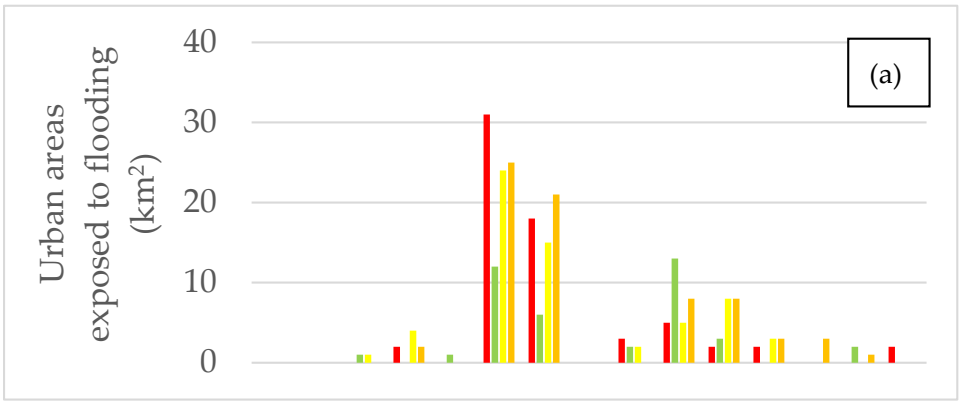

Figure 8. *Cont.*

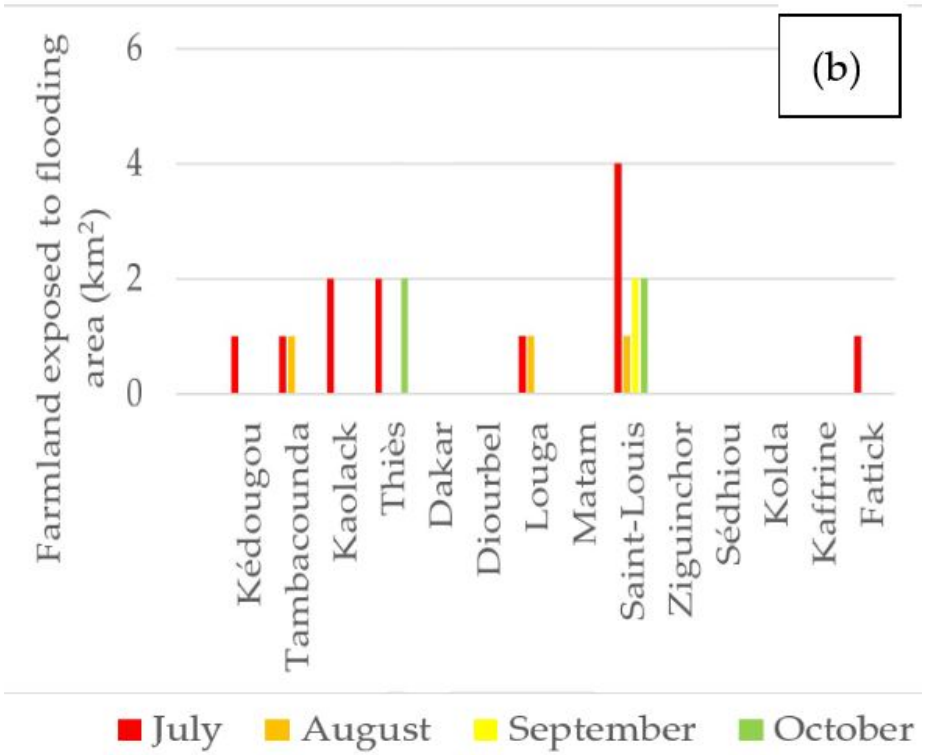

Figure 8. (**a**) Urban areas and (**b**) farmland exposed to flooding, derived from the intersection of MODIS land cover datasets with the flooded areas in the Google Earth Engine.

5. Discussion

Mapping flooded areas and assessing flooding exposure is particularly challenging in data-scarce regions like Senegal. Access to rapid, robust, and practical methodologies is crucial for flood mapping. In this study, we employed a remote sensing approach within the GEE framework. Our objectives were twofold: firstly, to integrate satellite imagery, GSW data, and HydroSHEDS data to identify the flooded areas for the 2022 flood event at the national scale, comparing them with hydrological and hydraulic modeling for a one-in-a-hundred-year flood event. Secondly, we aimed to evaluate flood exposure by population count, population density, urban area, and farmland area. By employing these methods, we have showcased the strengths and opportunities provided by the GEE platform for flood extent and flood exposure assessment.

5.1. Integrated Methodology for Flood Analysis

The detection of flooded areas involves processing satellite imagery within the Google Earth Engine (GEE) to identify changes in water coverage before and after flood events. This process is detailed in Section 3, where we explain the algorithms and data layers used. Studies, such as that by Cian et al. [38], utilize the Normalized Difference Flood Index (NDFI) to map flooded areas. Our method can be compared to these approaches that use flood indices to highlight improvements in terms of accuracy and efficiency.

In addition to satellite imagery analysis, our study uses the HEC-RAS 6.1 software with 2D geometry for hydrological and hydraulic modeling, employing the Soil Conservation Service (SCS) method to transform precipitation into runoff and the Barré de Saint-Venant equations for hydraulic propagation. This approach dynamically adjusts soil saturation and simulates water movement, accounting for momentum conservation, continuity, and flow resistance.

By integrating satellite imagery analysis within the GEE and centennial flood modeling, we provide a comprehensive quantification of the flooded area during the 2022 Senegalese extreme meteorological event. This integrated methodology leverages the

strengths of remote sensing and hydrological and hydraulic modeling, enhancing flood mapping accuracy and efficiency. Addressing the limitations of our approach will refine flood extent estimations through remote sensing and floodable areas by modeling for flood hazard assessment and mitigation strategy development and implementation, ultimately enhancing resilience to flood events.

While this combined approach enhances our understanding of flood dynamics, it has its limitations. The hydrological and hydraulic models' accuracy depends on the quality of the input data, such as the topography and land use class, and assumes homogeneity within grid cells (subject to varying resolution), which may not reflect the real-world variability [40].

5.2. Accuracy and Limitations of Flooded Area Mapping Using Sentinel-1 Imagery

Our study showcases the potential of flood mapping using Sentinel-1 data, coupled with the integration of global flood datasets like GSW, to achieve higher accuracy in estimating flooded areas compared to using optical, satellite-based datasets. Optical images often yield lower accuracy in delineating the extent of flooding due to issues such as cloud cover and a coarse revisit time (16 days). In contrast, Sentinel-1 satellite data offers advantages in identifying the extent of flooding due to radar transmission in the microwave spectrum, which remains unaffected by cloud cover, heavy rain, and low visibility, even operating at night [41,42]. However, it is worth noting that Sentinel-1 images may underestimate the flooding extent due to the spatial resolution (10 m), which may not be a sufficient resolution for flood extent quantification [11]. Nonetheless, at the (regional and national) scales in our study, these images can provide a satisfactory view of the problem. For local-scale assessments, we recommend considering radar images with much higher spatial resolutions, such as TerraSAR-X datasets [43], and comparing the results obtained with Sentinel-1 data. Despite Sentinel-1's relatively high temporal resolution (6 days), it may still underestimate flooded areas. More frequent (i.e., daily) satellite observations may become critical for more exhaustive mapping of the extent of flooding.

Temporal analysis of the extent of the flooding in all regions of Senegal during July, August, September, and October of the 2022 flood event reveals that the Saint-Louis [4] region experienced the most extensive flooding. This can likely be attributed to the combination of floodwater overflow from the Senegal river (Saint-Louis), potentially triggered by heavy rain, urban runoff, and rising groundwater.

The areas with the highest amount of flooding were observed in August 2022, a trend undoubtedly linked, at least in part, to the heavy rainfall recorded by the National Agency of Civil Aviation and Meteorology during August 2022. The total rainfall for August 2022 reached 105 mm, with an average daily rainfall of 3.36 mm, and a record single-day rainfall of 28.9 mm. Similar rainfall patterns were observed in the Saint-Louis [4] region, contributing to the extensive flooding there. While there was a strong correlation between rainfall and flooding, various contributing factors, such as infrastructure failures, pipeline blockages, the overflow of lakes, and the discharge of household septic tanks by the local population, were discussed previously by Sy et al. [5] in an earlier paper. These factors worsened the flood, by either increasing the quantity of water or obstructing the typical flow, for different locations and events.

5.3. Comparison of Remote Sensing Flood Extent and Flooding for a One-in-a-Hundred-Year Flood Event

We observed a lower level of agreement between the flooded areas derived in this study using Sentinel-1 data and those derived from the hydrological and hydraulic modeling conducted as part of the PGIIS project. This low level of agreement highlights both the strengths and limitations of satellite-based and modeling approaches. Our results from the GEE platform significantly deviate from the scenario corresponding to the flooding for a one-in-a-hundred-year flood event in terms of the flooded areas. However, by combining

the strengths and complementarity of the GEE platform (remote sensing observations over four months) and hydrological and hydraulic modeling (estimating flooding for a one-in-a-hundred-year flood event), stakeholders could benefit from an enhanced understanding of flood exposure, informing future risk assessments and risk management planning. Emphasis should be placed on regions such as Dakar [1], where the overlap between remote sensing and modeling is more significant. Targeted mitigation measures and the allocation of adequate resources in such regions are crucial.

Discrepancies between remote sensing and modeling results may arise due to several factors. The standard deviation σ of 2.49 in regard to the data overlap (1.34%) indicates a moderate level of variability, suggesting that while the model performs relatively consistently, there are noticeable differences in certain areas. The utilization of high-resolution DTM 2 m × 2 m data for hydraulic modeling may result in more precise floodable area delineation compared to remote sensing approaches. However, discrepancies may arise due to differences in data resolution and accuracy between remote sensing and hydraulic modeling inputs, particularly in areas with complex topography.

Hydrological and hydraulic models rely on various assumptions and parameterization techniques to simulate flood events accurately [44]. Differences in model assumptions, such as flood routing algorithms, Manning's roughness coefficients, and infiltration rates, may result in discrepancies between model predictions and observed flood extents from remote sensing data. Remote sensing data capture flood extents during specific time periods, providing snapshots of inundated areas. In contrast, hydraulic models simulate flood processes over time, considering factors such as rainfall duration, and antecedent soil moisture conditions. Temporal dynamics and the representation of flood processes in hydraulic models may influence flood extent predictions differently compared to remote sensing approaches.

Integrating remote sensing data with hydrological and hydraulic models can enhance the accuracy and reliability of flood extent predictions. Future research should focus on developing methodologies for assimilating remote sensing observations into model simulations to improve flood hazard mapping. Quantifying the uncertainties associated with remote sensing and modeling approaches is essential for effective flood risk management [45]. Understanding the sources of discrepancies and their implications can help stakeholders make informed decisions and prioritize mitigation measures in floodable areas. Further efforts should be made to harmonize and validate datasets from remote sensing and modeling approaches. Data fusion techniques, such as machine learning algorithms capable of analyzing large datasets to identify complex patterns contributing to flooding, regression models predicting relationships between weather variables and flood extent, classification models identifying at-risk areas based on historical flood patterns and current environmental conditions, and clustering algorithms grouping similar flood events to understand common characteristics and potential future occurrences, could be employed to integrate diverse datasets like satellite imagery, citizen science data, and weather data to potentially improve flood extent predictions.

5.4. Insights and Futures Implications for Flood Exposure Analysis

The combination of global databases on population distribution and density including GHLS datasets, along with updated land cover data from MODIS global land cover, provides great potential for assessing flood exposure in Senegal. Previous studies have indicated that increases in population exposure are mainly due to the increase in flooded areas and high-resolution datasets on population density [11,46]. In our study, Dakar [1] and Diourbel [3] are identified as the most exposed regions, not because they have the most extensive flooded areas, but due to their high population densities [31]. Dakar [1], being the capital of Senegal, and Diourbel [3], the religious region of the largest brotherhood in the country (Touba, in Senegal's Diourbel region, is a major religious hub as the headquarters of the influential Mouride Brotherhood. Its Great Mosque is one of Africa's largest, attracting

pilgrims nationwide, notably during events like the Grand Magal festival) are the most densely populated regions.

The population density in the GHLS datasets, used in this work, is based on the classification of building footprints from fine-scale satellite imagery, allowing for the distribution of the population over a smaller, more concentrated area. However, other databases, such as WorldPop, model a non-zero population density across almost the entire region, which means that the population is present in flooded areas. This may result in differences depending on the database used. Future work could improve estimates of the population exposed to flooding by further integrating national census data from the National Agency of Statistics and Demography [31]. The flood exposure results from this national census data, as well as from other global databases, can be compared with the results provided by GHLS datasets.

Furthermore, we could improve flood-exposed population estimates by incorporating social media population data [47]. Determining the exact percentage impact of incorporating social media population data on our flood exposure estimates would indeed require additional analyses. This would involve conducting thorough comparisons between the national census data, GHLS datasets, and social media population data.

The inclusion of social media data can significantly enhance our flood exposure estimates. This impact depends on various factors, such as the density and distribution of social media users in affected areas, and the quality and resolution of the social media data itself. By comparing the coverage, resolution, and accuracy of social media data with traditional data sources, we can provide a more precise estimate of its contribution. This assessment will help us understand how much more accurate our flood exposure estimates can become by integrating social media data.

In terms of flood exposure, absolute numbers provide an indication of the magnitude of an issue but lack context regarding its severity relative to the population size. Relative figures enable a comparison of exposure levels between different regions of Senegal, considering their respective population sizes. By considering relative figures, it becomes possible to identify the most exposed populations or regions in proportion to their size. Relative figures facilitate tracking changes in exposure over time, considering demographic growth or changes in population distribution. Considering both absolute and relative figures is crucial for a comprehensive assessment, leading to a more representative understanding of the extent of the hazard and potential exposure, therefore better informing decision-making for risk management actions.

As mentioned by authors such as Rentschler et al. [22], the results of estimations of population flood exposure cannot provide a complete picture of flood risk. Here, it is crucial to also consider the income levels of flood-exposed populations by region, as these can serve as proxies for people's vulnerability, capacity, and resilience. Vulnerability refers to the susceptibility to harm, capacity is the ability to mitigate and cope with floods, and resilience is the ability to recover from disasters.

For example, in the Dakar region [1], populations exposed to floods are more likely to have access to rapid government support systems post-disaster compared to those in regions like Kédougou [13] and Tambacounda [5]. Floods in low-income areas tend to have devastating and lasting impacts on livelihoods. Therefore, actions aimed at strengthening disaster prevention and recovery capacity are most urgently needed where low income and flood exposure coincide.

The total population in Senegal is expected to increase in the future [31], regardless of the population or flood dataset used. The increase in population exposure will primarily result from increases in the extent of flooding and changes in population growth, so we can expect increases in population exposure in the future. In any case, we could compare the findings of this population exposure study with future population exposure studies that incorporate 2030 estimation data to identify regions with slowing, continuing, or increasing flood exposure trajectories. This analysis may enable prioritization of adaptation measures

in regions where flood exposure has been growing or is expected to grow faster than the total population, especially under changing climate conditions.

The exposure of agricultural areas appears to be greatly underestimated by the MODIS dataset. This underestimation could be due to the spatial resolution of the data, but also to classification that is not verified by field studies. It is possible that agricultural areas are classified into other categories such as forests or others. Moreover, previous studies have shown that exposure estimated using this data is underestimated [11]. Therefore, it will be necessary in the future to find a method to verify this data, especially when working on a national scale.

6. Conclusions

This study presents a robust framework utilizing the GEE web platform for flood extent mapping and exposure assessment at both national and regional scales in Senegal. Our findings underscore the effectiveness of integrating radar satellite data with GWS and HydroSHEDS data, facilitating the mapping of flood extent over an extensive area of 196.722 km². The standard deviation (σ) of 2.49 for the data overlap (1.34%) indicates a moderate level of variability, suggesting that while the model performs relatively consistently, there are noticeable differences in certain areas due to differences in the data resolution, model assumptions, and temporal dynamics.

High-resolution DTM 2 m × 2 m data enhances the precision of hydrological and hydraulic modeling, but also introduces variability when compared to remote sensing data. Differences in flood routing algorithms, roughness coefficients, and temporal factors, further contribute to these discrepancies.

Our study emphasizes the potential of integrating water indices, machine learning, SAR data, time-series analysis, citizen science data, and data fusion techniques, to improve flood detection accuracy and efficiency. The generated flood extent maps and exposure assessments underscore the importance of developing a prioritization scheme for implementing flood mitigation and adaptation measures across diverse geographic regions.

Future research should focus on integrating remote sensing observations, citizen science data with hydrological and hydraulic models, validating datasets, and developing real-time flood monitoring systems. Creating user-friendly tools will facilitate broader adoption and utilization of flood extent information.

In conclusion, this study provides an efficient framework for flood risk hazard and exposure assessment in Senegal, offering valuable insights for flood mitigation efforts and contributing to the resilience of flood-prone communities.

Supplementary Materials: The following supporting information can be downloaded at: https://www.mdpi.com/article/10.3390/w16152201/s1, Table S1: Table representing the number of each region and the corresponding name of our study area. Table S2: Table listing flooded areas in km^2 per month by regions obtained by Google Earth Engine. Table S3: Table listing population exposed per month by regions obtained by Google Earth Engine. Table S4: Table listing urban exposed per month by regions obtained by Google Earth Engine.

Author Contributions: B.S. and F.B.B. conceived the original ideas. B.S., F.B.B. and H.D. drafted the original manuscript. B.S. and F.B.B. carried out data processing. B.S. and H.D. revised the original manuscript. All authors have read and agreed to the published version of the manuscript.

Funding: This research received no external funding.

Data Availability Statement: Most of the data are available on the Google Earth Engine platform. The code is available at https://code.earthengine.google.com/31f82fbef295dd8e2e4746dffea80174, accessed on 21 June 2024. The centennial modeling data were provided to us by submitting a request to PGIIS. For more information, please contact us.

Acknowledgments: The authors would like to thank Diadji Cisse, Hamidou Konate, and Martin Bortolotti for providing them with the data from the PGIIS project. The authors would also like to extend their sincere gratitude to Alana Weir from the Physical Volcanology Group at the University of Geneva for kindly reviewing the English language and providing valuable scientific insights.

Conflicts of Interest: The authors declare no conflicts of interest.

References

1. Ndehedehe, C. Hydro-Climatic Extremes: Climate change and human influence. In *Hydro-Climatic Extremes in the Anthropocene*; Springer International Publishing: Cham, Switzerland, 2023; pp. 25–55. [CrossRef]
2. UNISDR-CRED. *The Human Cost of Weather-Related Disasters 1995–2015*; The United Nations office for Disaster Risk Reduction (UNISDR) and Centre for Research on the Epidemiology of Disasters (CRED): Geneva, Switzerland, 2015; pp. 1–30.
3. EM-DAT. The OFDA/CRED International Disaster Database. Available online: https://public.emdat.be/data (accessed on 24 January 2024).
4. Chen, Y.; Zhou, H.; Zhang, H.; Du, G.; Zhou, J. Urban flood risk warning under rapid urbanization. *Environ. Res.* **2015**, *139*, 3–10. [CrossRef] [PubMed]
5. Sy, B.; Frischknecht, C.; Dao, H.; Consuegra, D.; Giuliani, G. Reconstituting past flood events: The contribution of citizen science. *Hydrol. Earth Syst. Sci.* **2020**, *24*, 61–74. [CrossRef]
6. de Moel, H.; Aerts, J.C.; Koomen, E. Development of flood exposure in the Netherlands during the 20th and 21st Century. *Glob. Environ. Chang.* **2011**, *21*, 620–627. [CrossRef]
7. Rahman, M.; Ningsheng, C.; Mahmud, G.I.; Islam, M.M.; Pourghasemi, H.R.; Ahmad, H.; Habumugisha, J.M.; Washakh, R.M.A.; Alam, M.; Liu, E. Flooding and its relationship with land cover change, population growth, and road density. *Geosci. Front.* **2021**, *12*, 101224. [CrossRef]
8. Hirabayashi, Y.; Mahendran, R.; Koirala, S.; Konoshima, L.; Yamazaki, D.; Watanabe, S.; Kim, H.; Kanae, S. Global Flood Risk under Climate Change. *Nat. Clim. Chang.* **2013**, *3*, 816–821. [CrossRef]
9. Kedowide, C.M.G.; Cissé, O. Adaptating to Flooding Impact in Yeumbeul Nord, a Suburb of Dakar, Senegal: Generation of Knowledge and of Mapping Data at the Crossroads of a Need for the Territorialization of Spatialized Phenomena. In Proceedings of the Resilient Cities, Bonn, Germany, 29–31 May 2014; pp. 1–20. Available online: http://hdl.handle.net/10625/53299 (accessed on 8 March 2024).
10. Waca. Floods in Senegal Are Retention Basins Part of the Solution? Available online: https://www.wacaprogram.org/article/floods-senegal-are-retention-basins-part-solution (accessed on 8 March 2024).
11. Li, C.; Dash, J.; Asamoah, M.; Sheffield, J.; Dzodzomenyo, M.; Gebrechorkos, S.H.; Anghileri, D.; Wright, J. Increased flooded area and exposure in the white Volta river basin in Western Africa, identified from multi-Source remote sensing data. *Sci. Rep.* **2022**, *12*, 3701. [CrossRef]
12. Sy, B. Approche Multidisciplinaire de l'évaluation de l'aléa d'inondation à Yeumbeul Nord, Dakar, Sénégal: La Contribution de La Science Citoyenne. Thesis, Université de Genève, Geneva, Switzerland, 2019. [CrossRef]
13. Muis, S.; Güneralp, B.; Jongman, B.; Aerts, J.C.; Ward, P.J. Flood Risk and Adaptation Strategies under Climate Change and Urban Expansion: A Probabilistic Analysis Using Global Data. *Sci. Total Environ.* **2015**, *538*, 445–457. [CrossRef]
14. DeVries, B.; Huang, C.; Armston, J.; Huang, W.; Jones, J.W.; Lang, M.W. Rapid and robust monitoring of flood events using Sentinel-1 and Landsat data on the Google Earth Engine. *Remote Sens. Environ.* **2020**, *240*, 111664. [CrossRef]
15. Ward, D.P.; Petty, A.; Setterfield, S.A.; Douglas, M.M.; Ferdinands, K.; Hamilton, S.K.; Phinn, S. Floodplain inundation and vegetation dynamics in the Alligator rivers region (Kakadu) of Northern Australia assessed uing optical and radar remote sensing. *Remote Sens. Environ.* **2014**, *147*, 43–55. [CrossRef]
16. Singha, M.; Dong, J.; Sarmah, S.; You, N.; Zhou, Y.; Zhang, G.; Doughty, R.; Xiao, X. Identifying floods and flood-affected paddy rice fields in Bangladesh based on Sentinel-1 imagery and Google Earth Engine. *ISPRS J. Photogramm. Remote Sens.* **2020**, *166*, 278–293. [CrossRef]
17. Gorelick, N.; Hancher, M.; Dixon, M.; Ilyushchenko, S.; Thau, D.; Moore, R. Google Earth Engine: Planetary-scale geospatial analysis for everyone. *Remote Sens. Environ.* **2017**, *202*, 18–27. [CrossRef]
18. Tiwari, V.; Kumar, V.; Matin, M.A.; Thapa, A.; Ellenburg, W.L.; Gupta, N.; Thapa, S. Flood inundation mapping-Kerala 2018; Harnessing the Power of SAR, Automatic threshold detection method and Google Earth Engine. *PLoS ONE* **2020**, *15*, e0237324. [CrossRef] [PubMed]
19. Moharrami, M.; Javanbakht, M.; Attarchi, S. Automatic Flood Detection Using Sentinel-1 Images on the Google Earth Engine. *Environ. Monit. Assess.* **2021**, *193*, 248. [CrossRef] [PubMed]
20. Johary, R.; Révillion, C.; Catry, T.; Alexandre, C.; Mouquet, P.; Rakotoniaina, S.; Pennober, G.; Rakotondraompiana, S. Detection of large-scale floods using Google Earth Engine and Google Colab. *Remote Sens.* **2023**, *15*, 5368. [CrossRef]
21. Ghouri, A.Y.; Khan, A.; Raoof, H.; Miandad, M.; Rehman, G. Flood mapping using the Sentinel-1 SAR dataset and application of the change detection approach technique (CDAT) to the Google Earth Engine in Sindh Province, Pakistan. *Ecol. Quest.* **2024**, *35*, 1–18. [CrossRef]
22. Rentschler, J.; Salhab, M.; Jafino, B.A. Flood exposure and poverty in 188 countries. *Nat. Commun.* **2022**, *13*, 3527. [CrossRef] [PubMed]
23. Van Den Homberg, M.; Susha, I. Characterizing data ecosystems to support official statistics with open mapping data for reporting on sustainable development Goals. *ISPRS Int. J. Geo-Inf.* **2018**, *7*, 456. [CrossRef]

24. Wouters, L.; Couasnon, A.; De Ruiter, M.C.; Van Den Homberg, M.J.; Teklesadik, A.; De Moel, H. Improving flood damage assessments in data-scarce areas by retrieval of building characteristics through UAV image segmentation and machine learning–a case study of the 2019 floods in Southern Malawi. *Nat. Hazards Earth Syst. Sci.* **2021**, *21*, 3199–3218. [CrossRef]
25. Cea, L.; Álvarez, M.; Puertas, J. Estimation of flood-exposed population in data-scarce regions combining satellite imagery and high resolution hydrological-hydraulic modelling: A case study in the Licungo Basin (Mozambique). *J. Hydrol. Reg. Stud.* **2022**, *44*, 101247. [CrossRef]
26. Mbow, C.; Diop, A.; Diaw, A.; Niang, C.I. Urban sprawl development and flooding at Yeumbeul suburb (Dakar-Senegal). *Afr. J. Environ. Sci. Technol.* **2008**, *2*, 75–88.
27. Sy, B.; Frischknecht, C.; Dao, H.; Giuliani, G.; Consuegra, D.; Wade, S.; Kêdowidé, C. Participatory approach for flood risk assessment: The case of Yeumbeul Nord (YN), Dakar, Senegal. *WIT Trans. Built Environ.* **2016**, *165*, 331–342. [CrossRef]
28. PGIIS. *Cartographie du risque d'inondation à l'échelle nationale*; Projet de Gestion Intégrée des Inondations au Sénégal (PGIIS): 2022; pp. 1–126.
29. ANACIM. *Rapport Annuel Du Groupe De Travail Pluridisciplinaire Pour La Campagne Agricole 2022*; Agence Nationale de l'Aviation Civile et de la Météorologie: Dakar, Senegal, 2022; pp. 1–41.
30. ANAT. *Atlas Cartographique*; Agence Nationale de l'Aménagement du Territoire: Dakar, Senegal, 2020; pp. 1–69.
31. ANSD. *5ème Recencement Général de La Population et de l'habitat*; Agence Nationale de la Statistique et de la Démographie: Dakar, Senegal, 2023; pp. 1–21.
32. ANSD. *Situation Économique et Sociale régionale*; Agence Nationale de la Statistique et de la Démographie: Dakar, Senegal, 2013; pp. 1–129.
33. Torres, R.; Snoeij, P.; Geudtner, D.; Bibby, D.; Davidson, M.; Attema, E.; Potin, P.; Rommen, B.; Floury, N.; Brown, M. GMES Sentinel-1 Mission. *Remote Sens. Environ.* **2012**, *120*, 9–24. [CrossRef]
34. Malenovský, Z.; Rott, H.; Cihlar, J.; Schaepman, M.E.; García-Santos, G.; Fernandes, R.; Berger, M. Sentinels for Science: Potential of Sentinel-1,-2, and-3 missions for scientific observations of ocean, cryosphere, and land. *Remote Sens. Environ.* **2012**, *120*, 91–101. [CrossRef]
35. Twele, A.; Cao, W.; Plank, S.; Martinis, S. Sentinel-1-Based Flood Mapping: A fully automated processing Chain. *Int. J. Remote Sens.* **2016**, *37*, 2990–3004. [CrossRef]
36. Clement, M.A.; Kilsby, C.; Moore, P. Multi-temporal synthetic aperture radar flood mapping using change detection. *J. Flood Risk Manag.* **2018**, *11*, 152–168. [CrossRef]
37. ESA. Revisit and Coverage Frequency of the Sentinel-1 Constellation, Showing Which Areas Are Mainly Covered with Descending or Ascending Imagery. Available online: Https://Sentinel.Esa.Int/Web/Sentinel/Copernicus/Sentinel-1/Acquisition-Plans (accessed on 24 January 2024).
38. Cian, F.; Marconcini, M.; Ceccato, P. Normalized Difference Flood Index for Rapid Flood Mapping: Taking Advantage of EO Big Data. *Remote Sens. Environ.* **2018**, *209*, 712–730. [CrossRef]
39. European Commission Global Human Settlement Layer—Open and Free Data and Tools for Assessing the Human Presence on the Planet. Available online: https://human-settlement.emergency.copernicus.eu/p2023Release.php (accessed on 22 April 2024).
40. Pappenberger, F.; Beven, K.; Horritt, M.; Blazkova, S. Uncertainty in the calibration of effective roughness parameters in HEC-RAS using inundation and downstream level observations. *J. Hydrol.* **2005**, *302*, 46–69. [CrossRef]
41. Amitrano, D.; Di Martino, G.; Iodice, A.; Riccio, D.; Ruello, G. Unsupervised rapid flood mapping using Sentinel-1 GRD SAR images. *IEEE Trans. Geosci. Remote Sens.* **2018**, *56*, 3290–3299. [CrossRef]
42. Nghia, B.P.Q.; Pal, I.; Chollacoop, N.; Mukhopadhyay, A. Applying Google Earth Engine for flood mapping and monitoring in the downstream Provinces of Mekong River. *Prog. Disaster Sci.* **2022**, *14*, 100235. [CrossRef]
43. Giustarini, L.; Hostache, R.; Matgen, P.; Schumann, G.J.-P.; Bates, P.D.; Mason, D.C. A Change detection approach to flood mapping in urban areas using TerraSAR-X. *IEEE Trans. Geosci. Remote Sens.* **2013**, *51*, 2417–2430. Available online: https://www.scopus.com/record/display.uri?eid=2-s2.0-84875707692&origin=inward&txGid=80f7a1beeeb5efc7c78e7e46e6626b75 (accessed on 22 June 2024). [CrossRef]
44. Ramírez, J.A. Prediction and Modeling of Flood Hydrology and Hydraulics. *Inland Flood Hazards Hum. Riparian Aquat. Communities* **2000**, 498.
45. Schulp, C.J.; Landuyt, D. Uncertainty measures and maps. In *Mapping Ecosystem Services*; Burkhard, B., Maes, J., Eds.; Pensoft Publishers: Sofia, Bulgaria, 2017; pp. 263–270. [CrossRef]
46. Smith, A.; Bates, P.D.; Wing, O.; Sampson, C.; Quinn, N.; Neal, J. New estimates of flood exposure in developing countries using high-resolution population data. *Nat. Commun.* **2019**, *10*, 1814. [CrossRef] [PubMed]
47. de Bruijn, J.A.; de Moel, H.; Jongman, B.; de Ruiter, M.C.; Wagemaker, J.; Aerts, J.C. A global database of historic and real-time flood events based on social media. *Sci. Data* **2019**, *6*, 311. [CrossRef] [PubMed]